Molecular Dynamics Simulations of the Photoactive Protein Nitrile Hydratase

Karina Kubiak and Wieslaw Nowak
Institute of Physics, Nicolaus Copernicus University, 87-100 Torun, Poland

ABSTRACT Nitrile hydratase (NHase) is an enzyme used in the industrial biotechnological production of acrylamide. The active site, which contains nonheme iron or noncorrin cobalt, is buried in the protein core at the interface of two domains, α and β. Hydrogen bonds between βArg-56 and αCys-114 sulfenic acid (αCEA114) are important to maintain the enzymatic activity. The enzyme may be inactivated by endogenous nitric oxide (NO) and activated by absorption of photons of wavelength $\lambda < 630$ nm. To explain the photosensitivity and to propose structural determinants of catalytic activity, differences in the dynamics of light-active and dark-inactive forms of NHase were investigated using molecular dynamics (MD) modeling. To this end, a new set of force field parameters for nonstandard NHase active sites have been developed. The dynamics of the photodissociated NO ligand in the enzyme channel was analyzed using the locally enhanced sampling method, as implemented in the MOIL MD package. A series of 1 ns trajectories of NHases shows that the protonation state of the active site affects the dynamics of the catalytic water and NO ligand close to the metal center. MD simulations support the catalytic mechanism in which a water molecule bound to the metal ion directly attacks the nitrile carbon.

INTRODUCTION

Biotechnology shows great promise for new ways of carrying out chemical reactions. A good example of the advantages of using microorganisms in chemistry is the synthesis of acrylamide (1). Since 1985, Japanese companies have used bacteria (*Rhodococcus* sp.) for the routine production of 30,000 ton/per year of this commodity (2–4). In this process bacterial enzyme nitrile hydratase (NHase) catalyses the hydration of nitriles to the corresponding amides (Fig. 1). Moreover, NHases are useful for the utilization of toxic pollutants and the production of pharmaceuticals, such as nicotinamide (vitamin PP) (4). Nowadays NHase from *Pseudomonas chlororaphis* B23 is applied in the production of acrylamide, which is widely used as a soil conditioner and in the production of paper, diapers, paints etc. (2). Conventional chemical synthesis of this compound, involving copper salts, leads to the formation of toxic by-products. In contrast, the microbial enzymatic synthesis is very safe and efficient (99.9% yield) (3,4). Unfortunately, the mechanism of the catalytic activity of NHases is not known (5–7) yet. To explain its activity, observed stereoselectivity, and photoactivation (8), a good understanding of NHase dynamics at the molecular level is required. The main obstacle in theoretical studies of NHases was the lack of reliable classical models, because the NHase active site is composed of nonstandard amino acids.

There are two types of NHases: iron and cobalt-containing NHases (Fe-type and Co-type NHase, respectively) (2,9,10). An interesting phenomenon is the photosensitivity of Fe-type NHases, which lose their activity after microbial incubation in dark conditions. In darkness the endogenous nitric oxide (NO) molecule is bound to the nonheme active center. The enzyme recovers its catalytic ability upon light irradiation (11,12). In dark conditions the Fe-N (NO) bond is extremely stable (12). Light irradiation not only breaks the Fe-N covalent bond but also induces local structural changes around the iron center (13). In particular, the arrangement of the so-called ''oxygen claw setting'' differs between active and inactive NHase forms (8). This phenomenon provokes an additional interest in NHases' properties.

All known NHases are composed of two subunits, α and β, and contain one metal atom (Fe or Co) per $\alpha\beta$ unit. (6,14–18). The metal center is located in the interior of a large cavity situated at the interface between the two subunits (6,14–18). A wide channel leads to this buried catalytic center. In the high resolution x-ray structure, only three water molecules located near the catalytic site are visible (15,19). The water molecules present at the interface of the two subunits and in the channel significantly contribute to the $\alpha\beta$ heterodimer formation (19). The water molecule (or a hydroxide ion) was proposed to participate in the catalytic reaction (14,19–21). Whether the catalytic water molecule is directly bound to the metal is still a matter of debate (5–7).

The crystal structure of Fe-type NHase from *Rhodococcus* sp. R312 (2.65 Å), first solved by Huang et al. (14), revealed a novel iron center with a structure of the ligand field composed of three sulfur atoms from cysteine residues (αCys-109, αCys-112, and αCys-114) and two amino nitrogen atoms from the protein backbone (αSer-113 and αCys-114). The next, x-ray structure (1.7 Å) has been resolved for NHase from *Rhodococcus* sp. N-771 by Nagashima et al. (15). These data, combined with the results of Fourier-transform ion cyclotron resonance mass spectrometry (FT-ICR MS) and high performance liquid chromatography (22), indicated that two coordinating cysteine residues are posttranslationally oxidized to the cysteine sulfenic and

Submitted July 23, 2007, and accepted for publication December 31, 2007.

Address reprint requests to Wieslaw Nowak, E-mail: wiesiek@fizyka.umk.pl; web site: http://www.phys.uni.torun.pl/~wiesiek.

Editor: Steven D. Schwartz.

0006-3495/08/05/3824/15 $2.00

doi: 10.1529/biophysj.107.116665

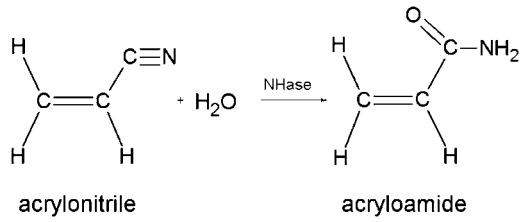

FIGURE 1 Reaction catalyzed by NHase.

cysteine sulfinic acids, αCys-114-SOH (αCEA114) and αCys-112-SO_2H (αCSD112), respectively. It has been shown that αCys-112 and αCys-114 are oxidized by atmospheric oxygen and that this posttranslational modification is essential for the catalytic activity of NHase (23). Furthermore, the oxygen atoms from αCys-112, αSer-113, and αCys-114 protrude from the plane containing the iron atom by 1.5 Å and form the oxygen claw setting (15). The structural function of this strange arrangements of atoms (Fig. 2) is still elusive. By the end of 2007, 16 x-ray structures of Fe and Co-type NHases had been solved (6,14–18).

There are a few proteins containing posttranslationally oxidized cysteines in the active site, such as reduced nicotinamide adenine dinucleotide peroxidase (24–26), peroxiredoxins (27–31), protein tyrosine phosphatase 1B (32), malate synthase (33), and cysteine sulfinic acid decarboxylase (34,35); but only NHases possess both Cys-SOH and Cys-SO_2H in the catalytic center. The biological role of such modifications is not explained yet. Both the inactive Fe-type NHase (12,21) and light active NHase (9,36) are in the low spin ferric state. In the active site of Co-type NHase, a low spin Co(III) ion is present (37,38).

Although several mimetic systems of the NHase active site have been investigated (39–45) and some theoretical models have been studied (13,46–55), the mechanism of hydration is unknown. The most often discussed are three alternative mechanisms proposed by Huang et al. (14). The metal acts as a Lewis acid in all these hypotheses. In the first mechanism (M1), a nitrile is directly coordinated to the metal. In the next step, a nucleophilic attack of water on the nitrile carbon occurs. In the other mechanisms (M2 and M3), it is postulated that a hydroxide ion is bound to the metal and then OH^- either attacks the nitrile carbon (M2) or activates some intermediate water, which in turn attacks the nitrile (M3). The distributions of waters in the NHase active site are important and so far have not been studied using dynamical methods. Static information on available water positions may be obtained from the recent nitrile/amide docking calculations performed by Peplowski et al. (56).

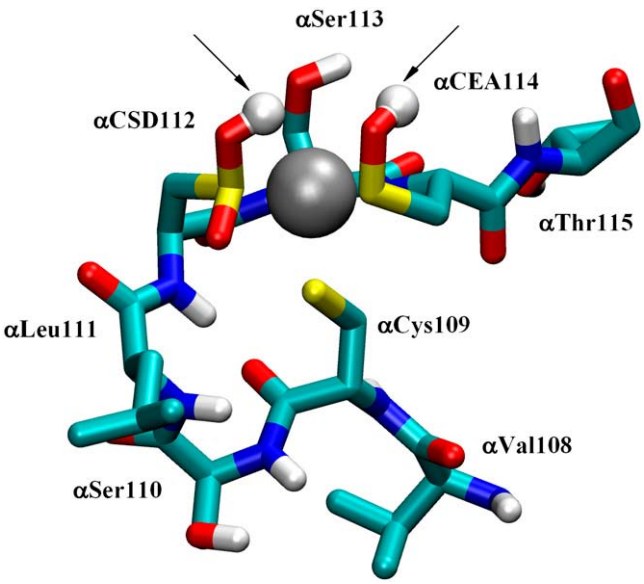

FIGURE 2 Structure of the BFE residue. Dissociating hydrogen atoms are indicated by arrows; residues forming the active site model are labeled.

The second poorly understood phenomenon is the photosensitivity of the Fe-type NHase. This question was previously investigated by Nowak et al. (13) using Density Functional Theory (DFT) method, but only a comparison of the DFT-optimized structures of 5- and 6-coordinated NHase active site models was presented. Substantial structural changes upon NO ligand binding to the iron center (''inverted doming'') may indicate that some mechanical signals are sent upon NO photodissociation. The photoactivation of NO-NHase requires that the blocking NO ligand leave the active site pocket. No NO transport routes in this enzyme interior have been described so far.

Here, for the first time, to our knowledge, classical molecular dynamics (MD) simulations for models of light-active (5-coordinated, **L**) and dark-inactive (6-coordinated, **D**) Fe-type NHase are presented. This is the first example, to our knowledge, of simulations for proteins containing such oxidized cysteines. Moreover, the locally enhanced sampling (LES) method (57) is used to determine NO diffusion paths in NHase. Since the protonation states of αCSD112 and αCEA114 residues seem to be crucial for the catalytic mechanism and NHase photosensitivity (13,48,56,58,59), we prepared classical trajectories for fully protonated (**LH2**, **DH2**) and doubly deprotonated (**L**, **D**) active site models. In the doubly deprotonated model (i.e., **L** or **D**), hydrogen atoms from both αCSD112 and αCEA114 side chains were dissociated.

The results here help in the understanding of the dynamical features of NHase and set some constrains on possible catalytic mechanisms, suggesting that a water molecule is directly bound to the iron ion. The dynamics of the active site channel, NO diffusion paths, and water molecules positions are key components in the functioning of this important industrial enzyme.

METHODS

The MD models of NHase active site

The novel models of NHase were constructed in the following way. The crystal structure of an inactive form isolated from *Rhodococcus* sp. N-771

(2AHJ) (15) was obtained from the Protein Data Bank (60). All minimizations, heatings, equilibrations, and dynamics runs were performed using the MOIL package (61). The MOIL force field, constructed as a hybrid of CHARMM, AMBER, and OPLS force fields, is well suited for protein simulations (62–64). The results were analyzed using MOIL-View (ver. 9.0) (65) software and the VMD code (ver. 1.8.3) (66). The active site of NHase (Fig. 2) contains four residues: αCys-109, αCSD112 (Cys-SO_2H), αSer-113, and αCEA114 (Cys-SOH). The central ion, Fe(III), is coordinated by the sulfur atoms of αCys-109, αCSD112, and αCEA114 and by the amide nitrogens of αSer-113 and αCEA114. The sixth coordinating position is occupied by NO, when present (forms **D**, **DH2**). To perform MD simulations a new, nonstandard ''residue'' called BFE was prepared as this active site model (Fig. 2). This fragment represents an extended environment of the Fe-type active site of NHase, so our model ''BFE residue'' additionally contains αVal-108, αSer-110, αLeu-111, and αThr-115.

It was necessary to add 68 new atom types to the standard MOIL force field (61). We used all the relevant properties of those atoms, e.g., masses, charges, and van der Waals parameters. To construct from them the BFE residue, the parameters for 76 bond lengths, 114 bond angles, 85 torsions, and 32 improper torsions were defined. The masses and van der Waals parameters of the atoms were the same as used in the MOIL force field. The atomic charges of αVal-108, αSer-110, αLeu-111, and αThr-115 were also standard. The geometry and charges of αCys-109, αCSD112, αSer-113, and αCEA114 residues were obtained from published (13) and additional DFT calculations performed at the level of B3LYP/6-31G(d,p) theory. Two cases were studied: fully protonated (**LH2**, **DH2**) and double-deprotonated (**L**, **D**) active site models. Deprotonation was realized by deleting hydrogen atoms from each of the CSD and CEA side chains. Detailed results of DFT/B3LYP/6-31G(d,p) calculations will be presented elsewhere. The DFT charges on the OH side group of αSer-113 were, however, lowered by 40% in the BFE model. This approach allowed us to reproduce the geometry of the active site observed in the crystal structure (15). The structure of the newly created BFE residue is shown in Fig. 2, and MOIL parameters for BFE are available in the Supplementary Material (Fig. S0 in Data S1).

The locally enhanced sampling method

The LES method developed by Elber and Karplus (57,67) is based on the assumption that the phase-space density of the molecular system can be written as a product of two parts:

$$\rho(P,Q,t) = \rho_S(P_S,Q_B,t)\rho_B(P_B,Q_B,t), \quad (1)$$

where ρ_S is the density of a small subsystem (NO ligands) and ρ_B is the density of the big subsystem (NHase protein). $\mathbf{R} = (\mathbf{P},\mathbf{Q})$ denotes the location of the system in the phase space of momenta $\mathbf{P}$ and space coordinates $\mathbf{Q}$. It is also assumed that the probability density of the protein can be written as

$$\rho_B(P_B,Q_B,t) = \delta(P_B - P_{0B}(t), Q_B - Q_{0B}(t)), \quad (2)$$

and the enhanced subsystem's density (N copies of NO ligand) can be written as

$$\rho_S(P_S,Q_S,t) = \sum_{k=1}^{N} w_k \delta(P_S - P_{0S}(t), Q_S - Q_{0S}(t)), \quad (3)$$

where w is a weight function (here $1/N$), and a complete set of Dirac δ functions is used for the expansion of densities. From these assumptions the equations describing motions of the protein and the copied system defined by Hamiltonian H are derived (67):

$$\frac{\partial Q_{0Sk}}{\partial t} = \frac{\partial H(P_{0Sk},Q_{0Sk},P_{0B},Q_{0B})}{\partial P_{0Sk}}$$
$$\frac{\partial P_{0Sk}}{\partial t} = -\frac{\partial H(P_{0Sk},Q_{0Sk},P_{0B},Q_{0B})}{\partial Q_{0Sk}} \quad (4)$$

$$\frac{\partial Q_{0B}}{\partial t} = \sum_{k=1}^{N} w_k \frac{\partial H(P_{0Sk},Q_{0Sk},P_{0B},Q_{0B})}{\partial P_{0B}}$$
$$\frac{\partial P_{0B}}{\partial t} = -\sum_{k=1}^{N} w_k \frac{\partial H(P_{0Sk},Q_{0Sk},P_{0B},Q_{0B})}{\partial Q_{0B}}. \quad (5)$$

The LES method as formulated in Elber and Karplus (57) has some drawbacks (68–72), i.e., temperatures of copies of the ligand may have been too high. However, we do not consider this a real problem in our study, since no thermodynamic quantities are calculated and a ligand heating in exploratory studies of conformational subspaces of proteins is an accepted technique (73,74). In our LES simulations a careful thermalization by velocity scaling was always assured.

The MD protocol

Hydrogen atoms were added using the *puth* module of MOIL (61). Then the protein was inserted into a 58 Å × 65 Å × 58 Å water box. All water molecules (>200) found in the x-ray structure were retained. The system was subjected to 10 ps water equilibration at 300 K (the protein was frozen) and then 3000 steps of minimization by the Powell method (75). Subsequently, the heating (10–300 K) step was carried out over 20 ps, followed by an equilibration at 300 K for 80 ps. Data were collected each 100 steps throughout the 1.0 ns period of the dynamics simulation. The temperature was held constant at 300 K by velocity scaling, and periodic boundary conditions were used. Cutoff distances for electrostatic and van der Waals interactions were 12 Å and 9 Å, respectively. To increase the time step to 1 fs, all bonds in the protein and all bonds and angles in water molecules were kept fixed by the SHAKE protocol (61). Since the solvent was explicitly introduced in the model, the dielectric constant was equal to one. In all 1 ns LES simulations, five copies of NO were employed.

RESULTS AND DISCUSSION

NHase stability

All calculations were performed for four models of NHase: a light-active fully protonated (**LH2**), a doubly deprotonated form (**L**), and the same two protonation states for the dark-inactive protein (**DH2**, **D**). First, the quality of our newly parametrized model of the active site (residue BFE) was checked. The root mean-square (RMS) deviation values between the crystal and minimized structures for the four models of NHase are listed in Table 1. The small RMS distances suggest that the protein structure is well preserved. However, the RMS value calculated for the residue BFE alone seems to be rather high. This number reflects a slightly modified orientation of αSer-113 side chain in the BFE model with respect to the conformation observed in the 2AHJ crystal. The Oγ atom forming the oxygen claw setting moves outward by ~1.5 Å, since it is stabilized by the hydrogen bond with the αThr-115 (data not shown). The presence of new hydrogen bonds, especially in the active site, indicates that αSer-113 may easily switch its orientation. Besides that, a small shift of iron ion of 0.2–0.3 Å toward the oxygen claw setting in all studied models is observed.

In all trajectories, the RMS plots level off after the initial phase of conformational changes; the protein does not lose its structure in the course of simulations. In the case of **L** and **LH2** forms, the average RMS values in the 1 ns trajectory are

TABLE 1 RMS values (in angstroms) between crystal and minimized structures of four models of NHase active site

	Protonated models		Deprotonated models	
Selection	LH2	DH2	L	D
Whole protein	0.39	0.38	0.43	0.42
Backbone only	0.26	0.26	0.30	0.30
Residue BFE	0.60	0.64	0.64	0.64

noticeable smaller than are those for **D** and **DH2** NHases (Fig. 3, and Fig. S1 in Data S1). Computer graphics analysis showed that the considerable contribution to the RMS distance comes from the relative motion of NHase subunits, the movement of the long N-terminal arm of the β-subunit, and conformational changes in the βPro-102–βVal-125 loop region. The mobility of this loop is fully understandable due to its position on the protein surface and is visible in the calculated fluctuations (see below). It is worth noting that the RMS distance calculated for the complete BFE residue in the **L** model is the lowest (Fig. 3, and Fig. S1 in Data S1) and equals 0.7 Å, so perhaps this is the preferred form of the enzyme.

Analysis of fluctuations

Time average fluctuations of atoms belonging to the same residue were calculated from the formula

$$fluc_k = \sum_{i=1}^{N} (\vec{r}_i^{\,k} - \langle \vec{r}_i^{\,k} \rangle_T)^2, \quad (6)$$

where $\vec{r}_i^{\,k}$ is the position of atom i in residue k and $\langle \vec{r}_i^{\,k} \rangle_T$ is the time-averaged position.

Large values of fluctuations correspond to flexible regions of the enzyme. The data calculated for the protein backbone in the 1 ns MOIL trajectories for the **L**, **D** and **LH2**, **DH2** models of NHase are presented in Fig. 4 and Fig. S2 in Data S1, respectively. The analysis of fluctuations contributes to the understanding of NHase architecture and may be linked to its catalytic function.

It is observed that the NO inactivation of the protonated enzyme model (i.e., a transition from **LH2** to **DH2**) leads to increased fluctuations (*red line*). The average fluctuations of **LH2** and **DH2** enzymes are ~0.611 Å^2 and 0.855 Å^2, respectively. The most flexible regions in the inactive **DH2** enzyme form are αGlu-48, a region from αAla-176 to αSer-182, βMet-69, βPhe-28, and a fragment βAsp-93–βPro-102; but in the **LH2** active NHase model only βVal-16 and βAsp-23 exhibit large fluctuations. The relatively high flexibility of the residues βVal-16, βAsp-23, and βPhe-28 is related to their location in the N-terminal arm of the β-subunit, rather than to some special functional role. Residues αAsp-37 and αGlu-48 belong to short helices H1 and H2, respectively. Fluctuations of ~1.8 Å^2 are probably affected by the absence of the first 13 residues in the model.

Significant fluctuations are observed in the loop region αPro-173–αSer-182: the difference between **LH2** (*black line*) and **DH2** (*red line*) of ~1 Å^2 is probably not related to NO dissociation since this loop is far away from the catalytic center. Further differences between fluctuations of the **LH2** and **DH2** models are in the βMet-69 and βAsp-93–βPro-102 regions. βMet-69 is located in the short loop connecting two surface helices, H3 and H4. These helices surround the channel entry, and their mobility probably reflects the relative subunit motions. Such motions were noticeably larger in the case of the **DH2** form of the enzyme (Fig. 3, and Fig. S2 in Data S1).

The side chain of αTyr-132 is located close to αVal-108, i.e., the first amino acid forming the BFE residue. In the **LH2**

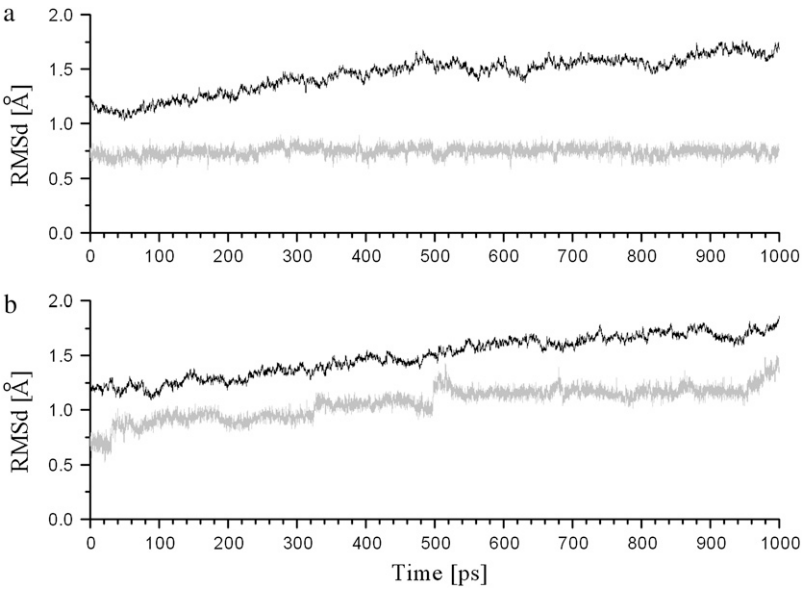

FIGURE 3 RMS distances in the 1 ns trajectories obtained for **L** (*a*) and **LH2** (*b*) models. Minimized structures were taken as the reference. The RMS distance for the protein backbone (*black line*) and the complete BFE residue (*shaded line*) are shown.

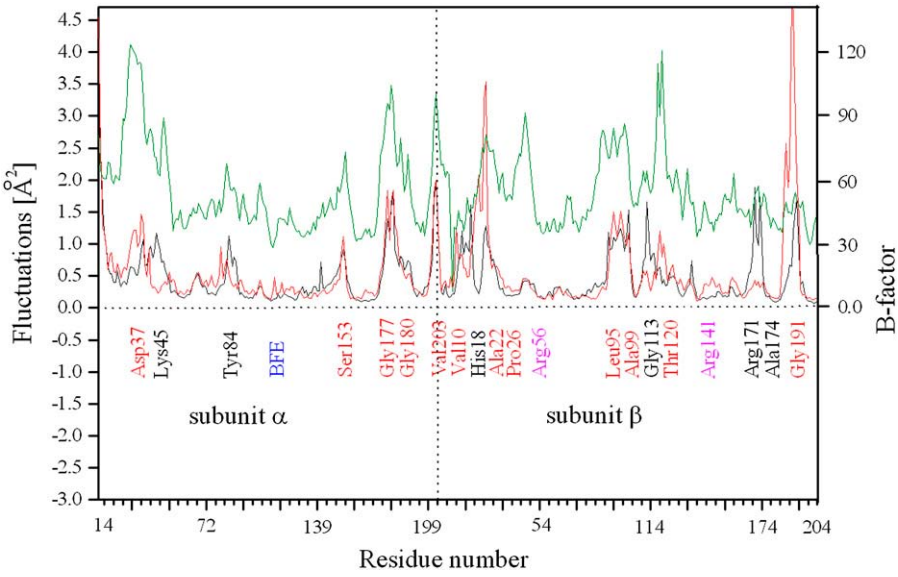

FIGURE 4 Average fluctuations in 1 ns trajectories calculated for deprotonated (**L** and **D**) models of the NHase active site. Values obtained for **L** are indicated in black and for the **D** form in red. The stand out and the crucial residues are labeled BFE; βArg-56 and βArg-141 residues are indicated by arrows. B-factor calculated from the crystal structure is indicated in green.

form the fluctuations of αTyr-132 are 0.897 Å^2, and in **DH2** fluctuations are only 0.303 Å^2. The distance between αVal-108 and αTyr-132 side chains in **DH2** is ~4 Å and remains constant during the 1 ns trajectory. In contrast, in the case of the **LH2** enzyme that distance varies from 5 Å to 10 Å. Such an effect could be induced by changes in the active site arrangement after the NO photodissociation.

Except for the H1 and H2 helices, the secondary structure elements are very well conserved. Generally, the fluctuations in the regions of α-helices and β-sheets of **LH2** and **DH2** are ~0.2–0.3 Å^2. An examination of the catalytically important residues, βArg-56 and βArg-141 (76), shows that their positions are quite stable (fluctuations vary from 0.2 Å^2 to 0.4 Å^2). Also the fluctuations of the BFE residue were quite small in both protonated models.

A similar analysis was performed for deprotonated **L** and **D** models (Fig. 4). Average fluctuations of the protein backbone were smaller than those in the protonated models: for **L** they were equal to 0.472 Å^2 and for **D**, 0.552 Å^2. The largest differences in the **L** and **D** flexibility were observed for the Asp-37, αLys-45, αArg-70, αTyr-84, βPro-26, βGly-113, βArg-171–βAla-174, and βGly-191 residues. In the regions of rather high fluctuations—αSer-153, αGly-177–αGly-180, αVal-203, βVal-10–βHis-18, and βLeu-95–βAla-99—the values calculated for **L** and **D** forms were similar. Such large values were expected: residues αSer-153 and αGly-177–αGly-180 are located in loops, αVal-203 caps the sequence of the α-subunit, and βVal-10–βHis-18 belong to the long βN-terminal arm. Amino acids βLeu-95–βAla-99 form the flexible helix H5. Again, also in deprotonated models, crucial arginine residues (76) are very rigid: their fluctuations are in the range of 0.13–0.26 Å^2.

In general, fluctuations are not much affected by the protonation state of oxidized cysteines from the active site. Both forms have fluctuations that are well correlated with experimental temperature B-factors measured for inactive form 2AHJ (*green line* in Fig. 4, and Fig. S2 in Data S1). However, the deprotonated model exhibits better correlations with experimental data shown in Fig. 4; so perhaps a deprotonated active site, as discussed in our earlier work (13), is present in the crystal (58).

Channels leading to the active sites in proteins are either ''tailor made'' or have rather random architectures and/or composition (77). The channel in Fe-NHase, lying at the interface between α- and β-subunits, is composed of 12 amino acids: αGln-90, αGlu-92, αTrp-117, αGlu-165, αArg-167, βMet-40, βPhe-41, βVal-44, βVal-52, βArg-56, βArg-141, (14,15), and βTyr-76. It is rather narrow, is ~12 Å long, and is located approximately along the axis perpendicular to the αCSD112, αCEA114, αSer-113 and Fe plane. It is rather hydrophilic: only 4 (out of 11) channel residues are hydrophobic. We have noticed that the channel structure is more rigid than the other fragments of NHase. The average fluctuations calculated for the channel residues are 52%, 66%, 39%, and 51% of the average fluctuations calculated for the **LH2**, **DH2**, **L**, and **D** forms, respectively. This observation indicates that the NHase channel architecture is protected. The rigidity comes mainly from the β-subunit, in which over 80% of amino acids forming channels are in α-helices (βH1, βH2). In the protonated forms, fluctuations of the channel residues are noticeably higher than in the deprotonated ones. We hypothesize that the lack of H-bonds—αCEA114-βArg-56/βArg-141 and αCSD112-βArg-141—increases flexibility of the $\alpha\beta$-subunit interface, which manifests itself in larger fluctuations of **LH2** and **DH2** forms in the channel region.

Fluctuations show that the presence (or absence) of an NO molecule in the studied system doesn't significantly affect the

dynamics of residues forming the channel. However, the modeling of NO dissociation slightly affects the structure of the BFE residue embedded in NHase. The conformation change upon the NO photodissociation is shown in Fig. 5. Low fluctuations of newly built, large residue BFE suggest that our selection of MOIL force field parameters was reasonable.

Functional hydrogen bonds

In the crystal structure of inactive NHase, several functionally important hydrogen bonds were observed in the catalytic center (14,15,76,78). We were able to identify the same interactions in our models and to check their role in the enzyme dynamics. It was found that the presence of these interactions depends on the protonation state of the NHase active site. For the **LH2** and **DH2** models, the oxygen atoms from αCSD112 and αCEA114 side chains did not participate in the hydrogen-bond interactions with either βArg-56 or βArg-141. However, in the 1 ns trajectory of the **L** form, the hydrogen bonds—Oδ (αCEA114)–βArg-56 and Oδ1 (αCSD112)–βArg-141—were extremely stable (Fig. 6). These bonds were not affected by the NO binding in the **D** form (Fig. S3 in Data S1). Moreover, in the **D** model of NHase another very stable hydrogen bond was identified: Oδ2 (αCSD112)–βArg-141 (Fig. S3 in Data S1). Thus, our data confirm that a reconstruction of experimentally observed spatial arrangement of hydrogen-bond forming atoms (14,15,76) in the NHase active site is possible for the deprotonated forms. We expect that during catalysis both, or at least one (58), αCSD112 and/or αCEA114 oxygen atoms are deprotonated.

It is worth noting that the observed donor-acceptor distance in the hydrogen bond is somewhat larger than a typical value. This is a feature of the MOIL force field. Hydrogen-bond distances and angles typical for the MOIL force field are summarized in Table 2.

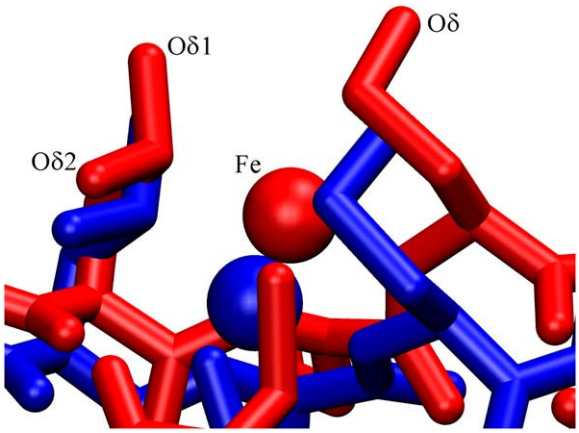

FIGURE 5 Changes in the catalytic center structure (deprotonated model) upon the NO photodissociation. The overlaid **L** and **D** models are indicated by red and blue, respectively. The NO molecule is not shown. The iron ion displacement is 1.48 Å, the Oδ (αCEA114) is 1.78 Å, the Oδ1 atom (αCSD112) is 1.06 Å, the Oδ2 atom (αCSD112) is 0.95 Å, and the sulfur atom from αCys-109 residue is 1.69 Å.

Since oxygen atoms Oγ (αSer-113), Oδ1 (αCSD112), and Oδ (αCEA114) form the oxygen claw setting (12,15), their geometries were monitored. In all trajectories, the distance between oxygen atoms Oδ1 (αCSD112) and Oδ (αCEA114) oscillated between 3.5–4.5 Å and was quite close to the distance of 3.4 Å measured in the crystal structure (15). However, the distances Oδ1–Oγ and Oδ–Oγ were ~2–3 Å longer than in the crystal (data not shown). This is connected with αSer-113 side-chain conformation change. This side chain deviates from its crystal orientation relative to the equatorial plane of the iron ion and is stabilized by a hydrogen bond with αThr-115.

NO dynamics

Tracing small ligands that travel inside a protein matrix provides data on transient cavities (57,79–81). The LES technique, despite some of its drawbacks (68–72), is particularly practical for this type of study, since energy barriers are lowered due to an approximate character of the Hamiltonian of the system under study. For **LH2** and **L** models, the diffusion of photodissociated NO within the NHase interior was monitored using a standard MD protocol (1 ns) and the LES approach with five copies of NO ligand (LES5). To some extent the NO molecule may be regarded as a very simplified model of NHase's natural ligand (acrylonitrile).

We observe that on a relatively short timescale of 5 ns (1 ns × 5 LES copies) the NO molecule can penetrate the active site cavity and the main NHase channel, but it does not leave the protein interior, except for one copy in the LES5 simulation (Fig. 7 *a*). In standard MD the sampling is more limited (Fig. 7 *b*). Despite the fact that the NO molecule is small, only one major diffusion path in the NHase interior was observed in our simulations.

In the initial phase, the qualitative picture of NO diffusion depends on the protonation state of the active site model. As shown in Fig. 8, the Fe-NO distance is larger in the **LH2** than in the **L** model. In the **LH2** trajectory after 500 ps, the NO molecule moves from the close vicinity of the active center to a transient docking site in the region of αGln-90, βMet-40, βVal-52, and βTyr-76 (Fig. 8 *a*). In the **L** model NO remains close almost the whole time to αTrp-117, βTyr-37, βMet-40, and βTyr-76, ~7 Å from the iron ion (Fig. 8 *b*).

It was postulated that the oxygen atoms from the oxygen claw setting (αCSD112, αSer-113, αCEA114) stabilizes the NO molecule in the inactive NHase form and probably plays an important role in the catalytic reaction (12,13,58,59). In our MD simulations, in both **L** and **LH2** models, the NO molecule leaves this pocket very easily. We do not observe any particular stabilization by the oxygen atoms. X-ray data suggested that positions of oxygen atoms from the post-translationally modified cysteines are stabilized by hydrogen

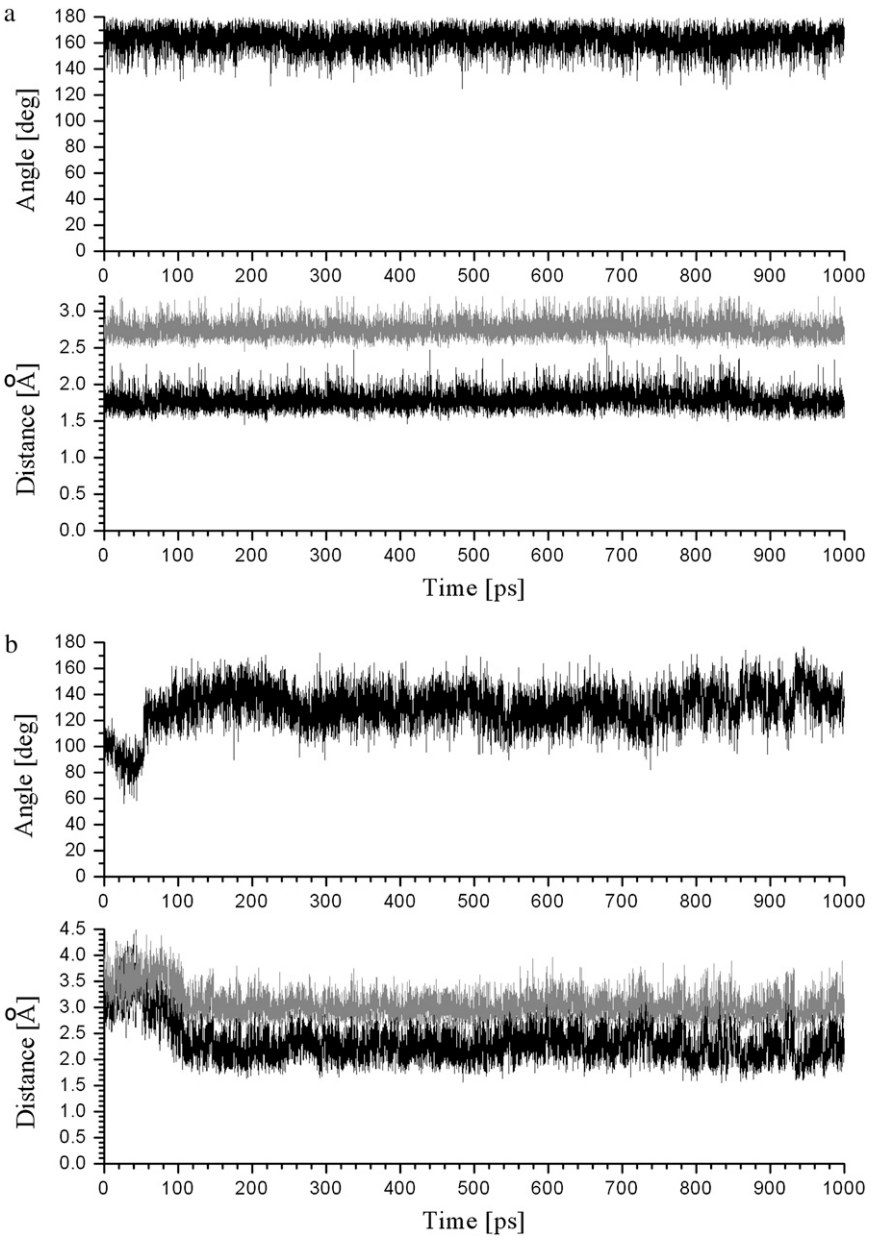

FIGURE 6 Hydrogen-bond interactions observed during 1 ns trajectories for the **L** NHase model: (*a*) αCEA114 (Oδ): βArg-56 (NH), and (*b*) αCSD112 (Oδ1): βArg-141 (NH). Distances hydrogen: acceptor (*black*), donor: acceptor (*gray*), and angles are shown.

bonds with βArg-56 and βArg-141 (14,15). Such H-bonds are also observed in our **L** and **D** trajectories.

The analysis of NO-protein atom collisions identifies the residues which may strongly affect ligand diffusion in NHase. If the distance measured between the nitrogen atom of NO molecule and any atom of the protein was smaller than 2.5 Å, the event was classified as a collision. Results are presented in Fig. 9 and Fig. S4 in Data S1. The strongest influence on NO mobility in the **L** model is from αGln-90, βTyr-37, βArg-56, and βTyr-76 and in the **LH2** model αGln-90, αTrp-117, βTyr-72, and βTyr-76 (Fig. S4, *a* and *b*, in Data S1). The same qualitative results were obtained for LES5 trajectories (Fig. 9). The listed residues form the channel (αGln-90, αTrp-117) or stabilize the channel (βTyr-37, βTyr-72) (19) or the active site (βArg-56) (14,76). It is worth noting that in all studied models the collision counts with βTyr-76 were the highest (except for some water molecules). This observation points to the βTyr-76 residue as a probable steric determinant of NHase catalytic activity. Very

TABLE 2 Average distances (angstroms) and bond angles (degrees) of the α-helices' and β-sheets' hydrogen bonds in the MOIL force field observed during the 1 ns trajectories for NHase

	Parameter		
	Distance H-acceptor	Distance donor-acceptor	Angle donor-H-acceptor
Literature (75)	1.80	2.7–3.1	180
Structure			
α-helix	1.97	2.91	156
β-sheet	1.97	2.87	160
Total	1.97	2.89	158

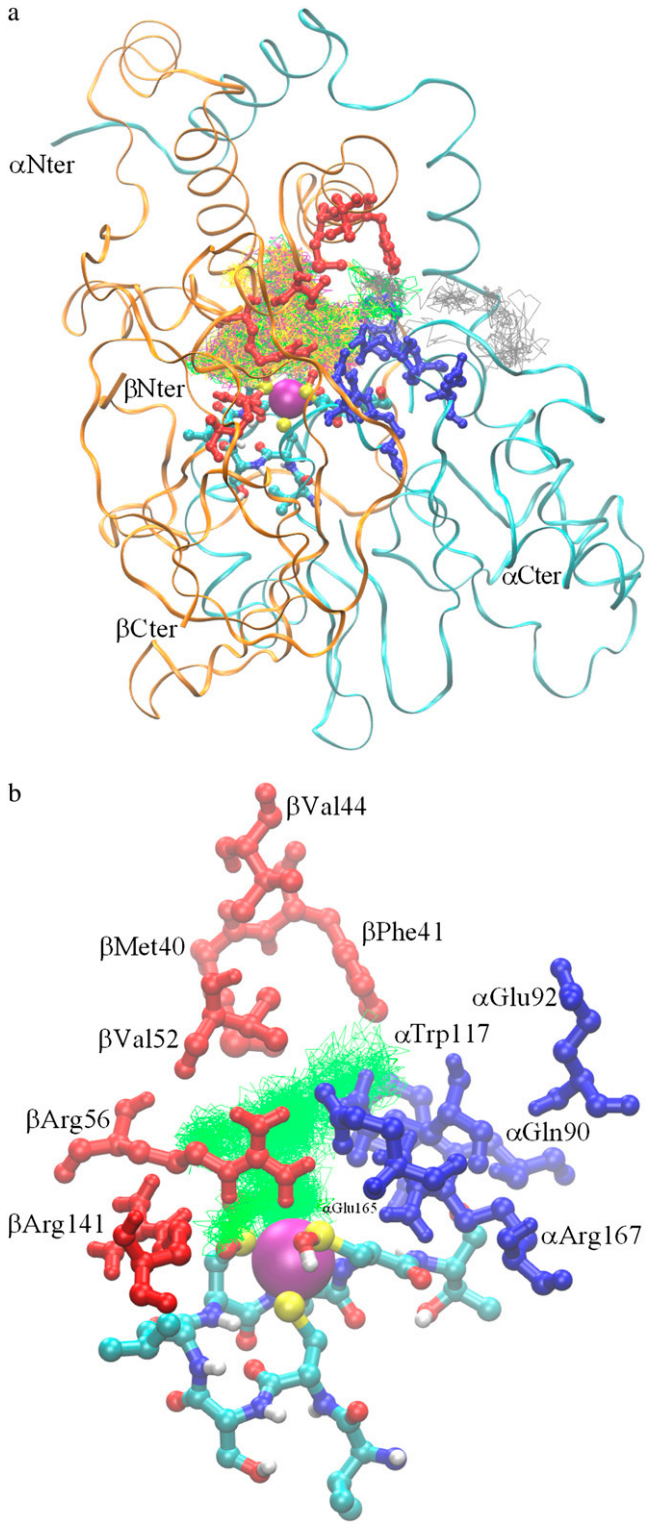

FIGURE 7 Trace of NO molecule in the NHase matrix for the L/LES5 model (*a*) and the LH2 model (*b*). Subunit α is indicated by cyan, subunit β by orange, residues from α- and β-subunit forming the channel walls are shown as blue and red CPK (Corey, Pauling, and Koltun atom representation), respectively. They are also labeled, as well as the N- and C-terminal ends of subunits. Iron ion is indicated by purple van der Waals sphere, active site as CPK colored by atom type (carbon atoms are *cyan*, nitrogen are *blue*, oxygen are *red*, hydrogen are *white*, and sulfur are *yellow*).

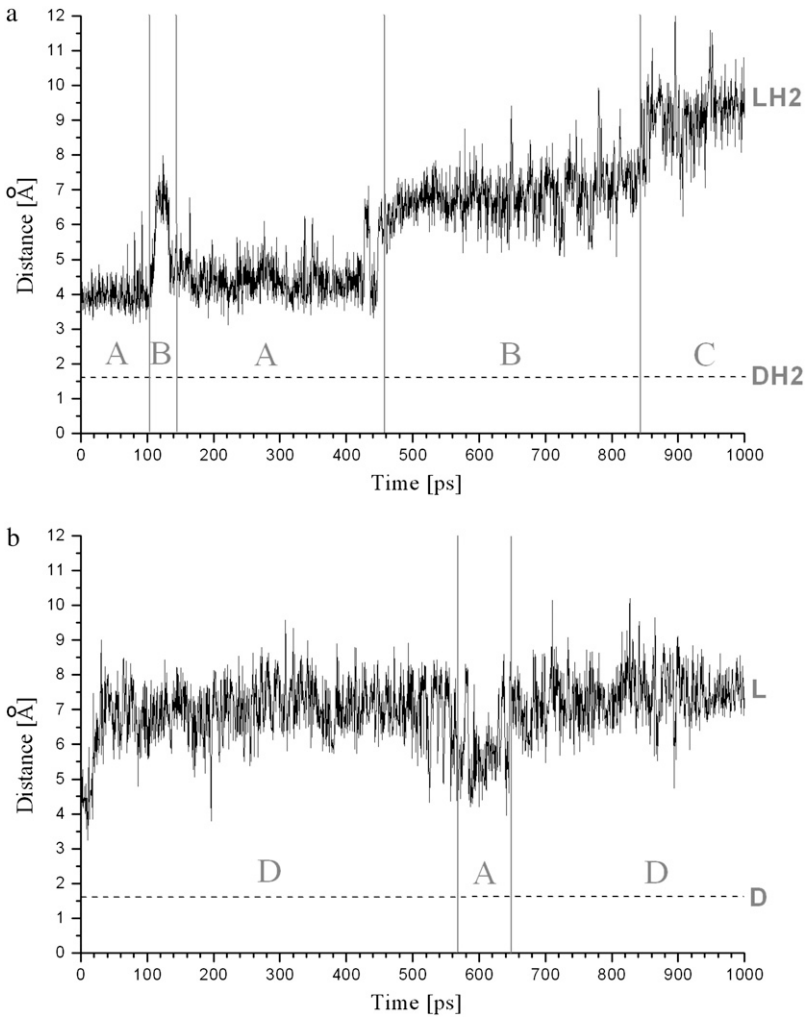

FIGURE 8 Distance between NO ligand and the center of the NHase active site observed in 1 ns trajectory for **LH2** (*a*) and **L** (*b*) models. Capitals indicate *A*, space up of active site; *B*, space surrounded by αGln-90, βMet-40, βVal-52, βVal-55, and βTyr-76; *C*, entrance from the channel; and *D*, space surrounded by αTrp-117, βTyr-37, βMet-40, and βTyr-76.

recently Mitra and Holtz (5) pointed out that the motif YYE(H/K)(W/Y) is strictly conserved among all known Co-NHases. In this region (β72–β76, in 2AHJ numbering) a similar motif YYERY for Fe-NHase is observed. Our βTyr-76 residue corresponds to the βTrp-72, a member of the αSer-112-βTyr-68-βTrp-72 catalytic triad postulated by these authors (5). This problem is investigated in our research group.

The noticeable collision count of βArg-56 indicates that this residue, known to be critical for the catalytic activity of NHase (76), may play a role in the proper orientation of the substrate. In pH conditions typical for the catalysis, the side chain of this residue is protonated (53). The nitrile has a strongly polarized $-C\equiv N$ group, and its negative end probably interacts with the NH_3^+ group from βArg-56. Thus the nitrile substrate is oriented exactly above the Fe-OH catalytic unit.

Collision histograms, presented in Fig. 9, and Fig. S4 in Data S1, clearly show that NO mainly contacts water molecules that are present in the channel. The most frequent collisions occur with ''crystallographic'' waters: for model **L**, TIP409-3000, for model **LH2**, TIP402-1200. Since in LES5 simulations NO travels closer to the bulk solvent, collisions with TIP3392 dominate in the **L/LES5** model (1100); but for the **LH2/LES5** system again collisions with a crystallographic water molecule, TIP473, dominate (4000).

Water dynamics and catalytic mechanism

The mechanism of catalytic activity of NHases is not known yet (5–7). There is consensus that the hydration reaction occurs near the metal ion center. The main difference in various hypothetical schemes is the location of the nitrile ligand (11). Some authors claim (5,9,44,82) that the nitrile is directly bound to the metal ion (M1) during catalysis, whereas others (6,20,51) assume that the substrate is rather localized above the oxygen claw setting and water is coordinated to the metal (M2, M3).

Spectroscopic data suggest that the sixth ligand in the free enzyme is either water (2,3,9,83) or hydroxide ion (20). There are experimental arguments that the sulfur coordination modulates the acidity of the metal-bound water and that perhaps metal-bound hydroxide is responsible for the hy-

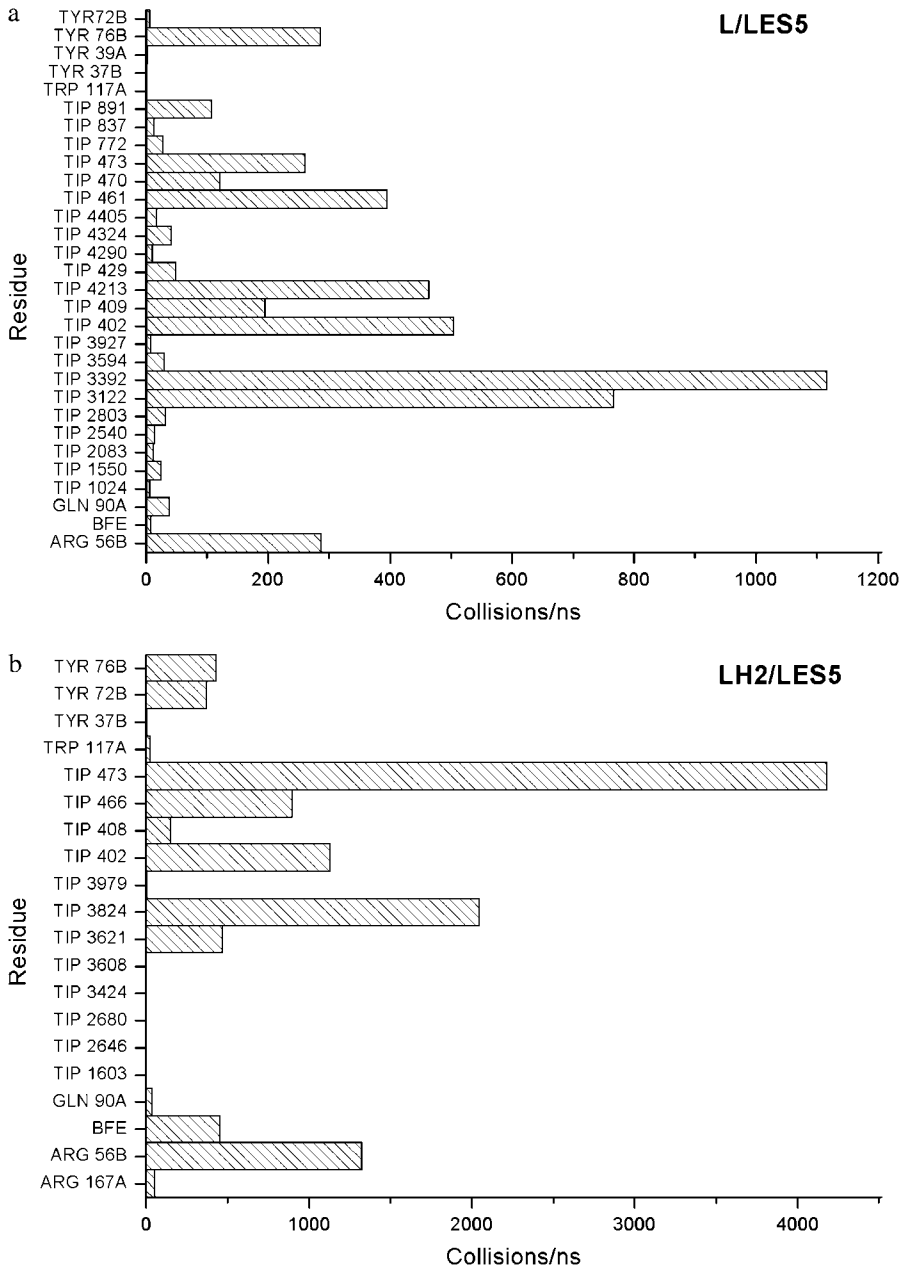

FIGURE 9 Histogram of the NO molecule collisions during the 1 ns trajectory obtained for LES trajectories for **L** (*a*) and **LH2** (*b*) form NHase active site models.

dration of nitriles (51,84,85). The alternative mechanism, in which nitriles coordinate to the metal by replacing water and subsequently are hydrolyzed, is not supported by studies of mimetic systems for the Co-NHase active site (51). Recent Fe-NHase (*Rhodococcus erythropolis* AJ270) x-ray structure indicates that a water molecule occupies the sixth ligand position even when the nitrile molecule is present (6).

On the other hand, studies on the synthetic Fe-NHase mimetic systems indicate that nitriles can reversibly bind to iron (44). This work lends validity to the proposed mechanism M1 in which the nitrile C≡N bond activation occurs via a coordinated Fe-NCR complex, since ligand exchange in a system resembling that of NHase is rapid (44).

Piersma et al. (76) have shown that the βArg-56Lys mutant has only 1% of catalytic activity of the native enzyme and βArg-56Glu and βArg-56Tyr variants are not active at all. The side chain of βArg-56 forms hydrogen bonds with αCEA114 (Fig. 10). In αGln-90Glu and αGln-90Asn mutants of Fe-NHase, k_{cat}, the kinetic constants, decreased to 24% and 5% of its wild-type value, respectively (78). These effects have been linked to the reorganization of the hydrogen-bond network involving water molecules (78). Based on mutational studies, Miyanaga et al. suggested that βTyr-68 of Co-NHase (corresponding to βTyr-72 of Fe-NHase) is probably involved in the stabilization of the imidate intermediate (18). The same Co-NHase from *Pseudonocardia Thermo-*

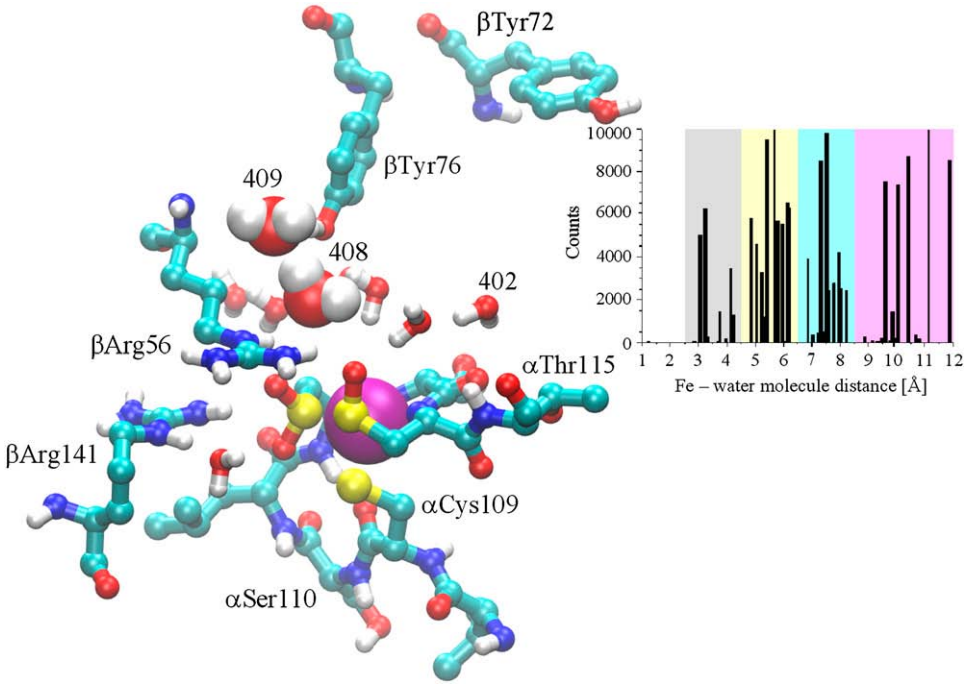

FIGURE 10 Water shell in the **L** model of the NHase active site. The iron ion is indicated by the purple van der Waals sphere; the active site and the most important residues (labeled) are shown as CPKs colored by atom type. Six water molecules creating the first water shell are also shown as CPKs; and two water molecules that are candidates for reactant waters (Tip408 and Tip409) are shown as van der Waals spheres and labeled. The αGln-90 residue is located above αThr-115. Distributions of water oxygen-Fe distances are shown in the inset. The purple box corresponds to channel waters.

philia JCM3095 was studied kinetically by Mitra and Holtz (5), who proposed that αSer-112-βTyr-68-βTrp-72 form the catalytic triad in that enzyme. In Fe-NHases the same roles might be played by αSer-113-βTyr-72-βTyr-76 residues. Interestingly in the Monte Carlo conformational study of acrylonitrile located in the Fe-NHase active site, Desai and Zimmer (82) found that βTyr-76 is one of the residues having the closest contacts with the nitrile.

Quantum-chemical studies have provided only limited information on a possible mechanism of the NHase catalytic activity (7,13,46,49,50,53,55). The most recent DFT/B3LYP calculations demonstrated that a simple coordination of the nitrile to the iron center does not sufficiently activate the ligand toward a nucleophilic attack of water (7). The low spin Fe^{3+} iron center is weak Lewis acid. The activation of water by the deprotonated αCEA114 residue leads to the first-shell mechanism with the energy barrier of 20.2 kcal/mol (7), which is still above experimental estimates of 13–15 kcal/mol (18,78).

The role of water in the catalytic mechanism is widely discussed (5,6,14,20,44,47,58,78). There is evidence that a few water molecules are present in the closest neighborhood of the active center (9,19,58). However, only static locations of hydrogen-bonded water molecules have been considered so far. We have investigated water dynamics in the NHase active and inactive form interiors. All water molecule-Fe^{3+} distances were monitored and analyzed. Our results suggest that water molecules can easily get into the active site from the bulk solvent. For example, out of 20–25 water molecules present in the NHase channel or active site cavity, some 6–7 molecules snaked in from the bulk during 1 ns of MD. We also observed multiple water molecule exchanges in the main channel. In general, our observations that the water molecules easily penetrate the NHase channel and fill the space located close to the metal ion are in agreement with the composition of this region: out of 11 amino acids 5 are charged, i.e., strongly hydrophilic.

Internal water molecules seem to be organized in several ''layers'' (*inset* in Fig. 10). In the active NHase models **L** and **LH2**, the sixth coordination position is occupied most of the time by a water molecule which had arrived from the exterior. In the range of 6 Å from the Fe^{3+} ion ~10 water molecules are located. Usually 1–2 water molecules are easily exchangeable. Other water molecules stabilize αCys-109, αLeu-111 (hydrogen bonds to amide nitrogen atoms), αCEA114, or αThr-115 residues (hydrogen bonds to carbonyl oxygen atoms). The hydrogen-bond network is closely related to that described by Takarada (78). Near βTyr-76, a cluster of three water molecules was observed in all trajectories (Fig. 10). These water molecules are quite labile and probably define a path for the water to reach the active site.

Searching for a water molecule which might attack a nitrile substrate and/or exchange positions with the catalytic water, we analyzed NO-water collision counts (Fig. 9 and Fig. S4 in Data S1). In this analysis, we assumed that the NO molecule is a crude model of the nitrile. In our standard MD trajectories, water TIP402 (no. 195 in 2AHJ), located close to αGln-90, participates in over 50% of NO-water collisions in **LH2** and is the probable candidate for the hydration water. In LES5 trajectories this molecule also has a high collisions count (Fig. 9). The other candidate is water TIP408, which is located mainly in the central part of the oxygen claw setting, 5–6 Å away from Fe^{3+} or bound to βTyr-76 and βTyr-72. The maxima in collision counts observed in Fig. 9 *a*

(TIP3302) and Fig. 9 *b* (TIP473) correspond to water molecules coordinated directly to the Fe^{3+} ion. We found that in the absence of a substrate the catalytic water belongs to the first water shell (mechanism M2).

Candidates for catalytically important waters are shown in Fig. 10. It is worth noting that the TIP409 water, located in the second ''layer'' of waters, is quite localized due to steric interactions with βMet-40 and βTyr-76. One can see from Fig. 9 *a* that such a molecule blocks an exit of NO from the cavity and has a good chance to react with an activated nitrile, if the nitrile was bound directly to the Fe center (step 1 in mechanism M1 proposed in Huang et al. (14)). On the other hand, the position of water TIP408 (Fig. 10) suggests that this molecule may participate in a nucleophilic attack on the nitrile activated by the Fe-bound hydroxide ion (M2) or smoothly replace any hydroxide ion bound to the Fe ion (a step required in mechanisms M2 and M3 (14)).

Interestingly, in the **LH2** model a NO-water exchange phenomenon was observed. At 448 ps one of the water molecules moved toward the iron ion from ~6 Å to ~2 Å. At the same moment the NO molecule left the closest neighborhood of the iron ion (Fig. 11). This exchange suggests that the endogenous NO molecule bound to the iron in the inactive form of NHase may easily photodissociate, thus activating the enzyme (12). There are no mechanical obstacles preventing such reactions.

Preliminary amide/nitrile docking studies have provided support for the mechanism M2, in which metal activated water (or hydroxide ion) performs a direct attack on the nitrile carbon (56). Our data on the water dynamics further support this hypothesis. However, the presence of an imidate intermediate is suggested by recent quantum chemical DFT calculations of reaction paths (7,86).

CONCLUSIONS

NHases from *Rhodococuss* sp. and related bacteria are key ''workhorses'' in the green production of amides. Once their catalytic activity is fully understood, NHases may be genetically tuned for safe and cheap production of other useful chemicals. The parametrization of the Fe-NHase active site for the MOIL force field (61) has been developed, which made the

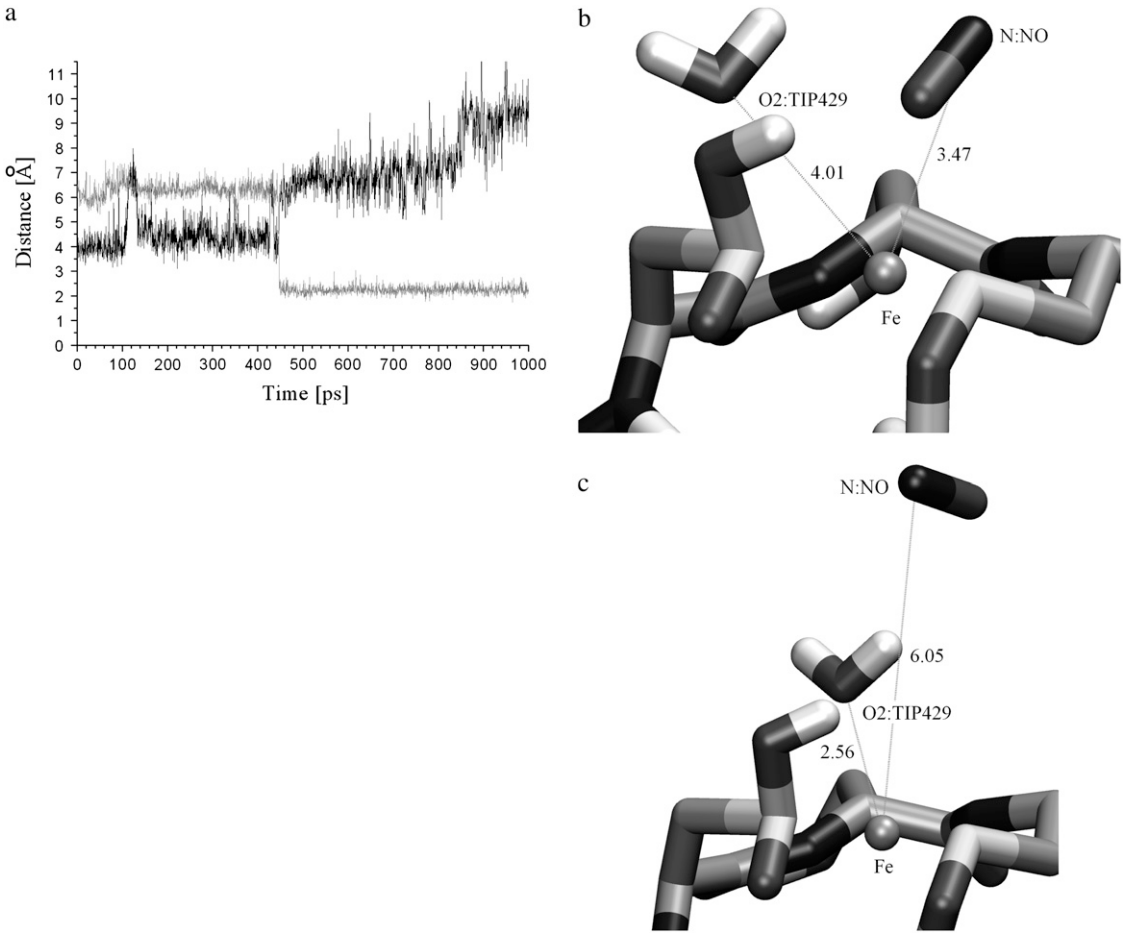

FIGURE 11 Exchange of the water and NO molecules in the 1 ns trajectory calculated for light-active NHase with the protonated active site. (*a*) The distance Fe-N (NO) (*black*) and the Fe-water molecule (*gray*). (*b*) Arrangement of the NO and water molecule (in respect to the iron ion) before exchange (446.8 ps) and (*c*) after exchange (448 ps).

MD studies of a new group of enzymes possible. Moreover, for the first time, to our knowledge, MD parameters for post-translationally oxidized cysteines have been proposed. Such residues have been discovered recently (24–35) in many enzymes, so the new parameters open the way for their modeling.

The MD simulation of an active NHase (**L** form) and NO inactivated (**D** form) with a deprotonated active site provided insights into the characteristics of the NHase catalytic center, the main channel stability, the NO diffusion process, and water dynamics. The effects of protonation states of CSD and CEA residues on NHase dynamics were studied. In the protonated forms, fluctuations of the channel residues are higher than in the deprotonated ones. The lack of H-bonds αCEA114-βArg-56/βArg-141 and αCSD112-βArg-141 in **LH2** and **DH2** increases flexibility of the $\alpha\beta$-subunit interface. Analysis of fluctuations (1 ns trajectories) shows that the main ligand's entry/exit channel is stiffer than the average regions of NHase. Calculated fluctuations correlate well with the experimental temperature B factors, supporting the good quality of our model.

The photodissociated NO, according to 1 ns simulations with the LES method, shows that only one way outside is possible through the main channel. The NO collisions count analysis indicated residues βTyr-76 and βArg-56 as possible steric factors in nitrile/amide diffusion. The oxygen claw setting (14) does not stabilize free NO, but its structure is affected by the propensity of αSer-113 for H-bond formation with αThr-115. If it is not an artifact, this effect should be further studied. The kinetics of NO photodissociation is currently being investigated within the Landau-Zener model (87,88) using the newly developed parameters.

MD simulations show that both in the channel and in proximity to the active site there are two water layers. We found that the exchange of water positions is easy. On a 1 ns timescale, even exchange of water with NO trapped in an oxygen claw setting is possible. The water flow is particularly intensive in the region of βTyr-76. The dynamical spatial arrangement of water molecules in the Fe-NHase active site, the NO diffusion paths, and the hydrogen-bonds network and its relation to mutational studies' data support the catalytic mechanism M2 proposed by Huang et al. (14). In this scheme the hydroxide ion coordinated to Fe^{3+} activates nitrile, and the second layer of water performs a nucleophilic attack on the nitrile carbon. This reaction may go through the imidate intermediate (7,56). The proper arrangement of nitrile is probably warranted by electrostatic interaction with the βArg-56 residue. That is why βArg-56 is so important for NHase activity. Further studies with nitriles and Car-Parinello-type quantum dynamics calculations are needed to completely rule out other alternatives.

SUPPLEMENTARY MATERIAL

To view all of the supplemental files associated with this article, visit www.biophysj.org.

The authors thank Lukasz Peplowski for his help in the parametrization of BFE.

This work was supported by the Polish budget funds for science, grant No. 2P04A07229 and grant No. UMK-377-F.

REFERENCES

1. Thomas, M. T., R. DiCosimo, and V. Nagarajan. 2002. Biocatalysis: applications and potentials for the chemical industry. *Trends Biotechnol.* 20:238–242.
2. Kobayashi, M., T. Nagasawa, and H. Yamada. 1992. Enzymatic synthesis of acrylamide: a success story not yet over. *Trends Biotechnol.* 10:402–408.
3. Yamada, H., and M. Kobayashi. 1996. Nitrile hydratase and its application to industrial production of acrylamide. *Biosci. Biotechnol. Biochem.* 60:1391–1400.
4. Yamada, H., S. Shimizu, and M. Kobayashi. 2001. Hydratases involved in nitrile conversion: screening, characterization and application. *Chem. Rec.* 1:152–161.
5. Mitra, S., and R. C. Holz. 2007. Unraveling the catalytic mechanism of nitrile hydratases. *J. Biol. Chem.* 282:7397–7404.
6. Song, L., M. Wang, J. Shi, Z. Xue, M.-X. Wang, and S. Qian. 2007. High resolution x-ray molecular structure of the nitrile hydratase from *Rhodococcus erythropolis* AJ270 reveals posttranslational oxidation of two cysteines into sulfinic acids and a novel biocatalytic nitrile hydration mechanism. *Biochem. Biophys. Res. Commun.* 362:319–324.
7. Hopmann, K. H., J.-D. Guo, and F. Himo. 2007. Theoretical investigation of the first-shell mechanism of nitrile hydratase. *Inorg. Chem.* 46:4850–4856.
8. Endo, I., M. Odaka, and M. Yohda. 1999. An enzyme controlled by light: the molecular mechanics of photoreactivity in nitrile hydratase. *Trends Biotechnol.* 17:244–248.
9. Sugiura, Y., and J. Kuwahara. 1987. Nitrile hydratase: the first non-heme iron enzyme with a typical low-spin Fe(III)-active center. *J. Am. Chem. Soc.* 109:5848–5850.
10. Brennan, B. A., J. G. Cummings, D. B. Chase, I. M. Turner, and M. J. Nelson. 1996. Resonance Raman spectroscopy of nitrile hydratase, a novel iron-sulfur enzyme. *Biochemistry.* 35:10067–10077.
11. Noguchi, T., J. Honda, T. Nagamune, H. Sasabe, Y. Inoue, and I. Endo. 1995. Photosensitive nitrile hydratase intrinsically possesses nitric oxide bound to the non-heme iron centre: evidence by Fourier transform infrared spectroscopy. *FEBS Lett.* 358:9–12.
12. Odaka, M., K. Fuji, M. Hoshino, T. Noguchi, M. Tsujimura, S. Nagashima, M. Yohda, T. Nagamune, Y. Inoue, and I. Endo. 1997. Activity regulation of photoreactive nitrile hydratase by nitric oxide. *J. Am. Chem. Soc.* 119:3785–3791.
13. Nowak, W., Y. Ohtsuka, J. Hasegawa, and H. Nakatsuji. 2002. Density functional study on geometry and electronic structure of nitrile hydratase active site model. *Int. J. Quantum Chem.* 90:1174–1187.
14. Huang, W., J. Jia, J. Cummings, M. Nelson, G. Schneider, and Y. Lindqvist. 1997. Crystal structure of nitrile hydratase reveals a novel iron centre in a novel fold. *Structure.* 5:691–699.
15. Nagashima, S., M. Nakasako, N. Dohmae, M. Tsujimura, K. Takio, M. Odaka, M. Yohda, M. Kamiya, and I. Endo. 1998. Novel non-heme iron centre of nitrile hydratase with a claw setting of oxygen atoms. *Nat. Struct. Biol.* 5:347–351.
16. Miyanaga, A., S. Fushinobu, K. Ito, and T. Wakagi. 2001. Crystal structure of cobalt-containing nitrile hydratase. *Biochem. Biophys. Res. Commun.* 288:1169–1174.
17. Nakasako, M., M. Odaka, M. Yohda, N. Dohmae, K. Takio, N. Kamiya, and I. Endo. 1999. Tertiary and quaternary structures of photoreactive Fe-type nitrile hydratase from *Rhodococcus* sp. N-771: roles of hydration water molecules in stabilizing the structures and the structural origin of the substrate specificity of the enzyme. *Biochemistry.* 38:9887–9898.

18. Doan, P. E., M. J. Nelson, H. Jin, and B. M. Hoffman. 1996. An implicit TRIPLE effect in mims pulsed ENDOR: a sensitive new technique for determining signs of hyperfine couplings. *J. Am. Chem. Soc.* 118:7014–7015.
19. Scarrow, R. C., B. S. Strickler, J. J. Ellison, S. C. Shoner, J. A. Kovacs, J. G. Cummings, and M. J. Nelson. 1998. X-ray spectroscopy of nitric oxide binding to iron in the inactive nitrile hydratase and a synthetic model compound. *J. Am. Chem. Soc.* 120:9237–9245.
20. Tsujimura, M., N. Dohmae, M. Odaka, M. Chijimatsu, K. Takio, M. Yohda, M. Hoshino, S. Nagashima, and I. Endo. 1997. Structure of the photoreactive iron center of the nitrile hydratase from *Rhodococcus* sp. N-771. *J. Biol. Chem.* 272:29454–29459.
21. Murakami, T., M. Nojiri, H. Nakayama, M. Odaka, M. Yohda, N. Dohmae, K. Takio, and T. Nagamune. 2000. Post-translational modification is essential for catalytic activity of nitrile hydratase. *Protein Sci.* 9:1024–1030.
22. Hourai, S., M. Miki, Y. Takashima, S. Mitsuda, and K. Yanagi. 2003. Crystal structure of nitrile hydratase from a thermophilic *Bacillus smithii*. *Biochem. Biophys. Res. Commun.* 312:340–345.
23. Miyanaga, A., S. Fushinobu, K. Ito, H. Shoun, and T. Wakagi. 2004. Mutational and structural analysis of cobalt-containing nitrile hydratase on substrate and metal binding. *Eur. J. Biochem.* 271:429–438.
24. Ahmed, S. A., and A. Claiborne. 1992. Active-site structural comparison of streptococcal NADH peroxidase and NADH oxidase. Reconstitution with artificial flavins. *J. Biol. Chem.* 267:3832–3840.
25. Stehle, T., A. Claiborne, and G. E. Schulz. 1993. NADH binding site and catalysis of NADH peroxidase. *Eur. J. Biochem.* 211:221–226.
26. Poole, L. B., A. Karplus, and A. Claiborne. 2004. Protein sulfenic acids in redox signaling. *Annu. Rev. Pharmacol. Toxicol.* 44:325–347.
27. Chae, H. Z., K. Robison, L. B. Poole, G. Church, G. Storz, and S. G. Rhee. 1994. Cloning and sequencing of thiol-specific antioxidant from mammalian brain: alkyl hydroperoxide reductase and thiol-specific antioxidant define a large family of antioxidant enzymes. *Proc. Natl. Acad. Sci. USA.* 91:7017–7021.
28. Chae, H. Z., S. J. Chung, and S. G. Rhee. 1994. Thioredoxin-dependent peroxide reductase from yeast. *J. Biol. Chem.* 269:27670–27678.
29. Wood, Z. A., L. B. Poole, and P. A. Karplus. 2003. Peroxiredoxin evolution and the regulation of hydrogen peroxide signalling. *Science.* 300:650–653.
30. Wong, C., K. Siu, and D. Jin. 2004. Peroxiredoxin-null yeast cells are hypersensitive to oxidative stress and are genomically unstable. *J. Biol. Chem.* 279:23207–23213.
31. Sayed, A. A., and D. L. Williams. 2004. Biochemical characterization of 2-Cys peroxiredoxins from Schistosoma mansoni. *J. Biol. Chem.* 279:26159–26166.
32. van Montfort, R. L. M., M. Congreve, D. Tisi, R. Carr, and H. Jhoti. 2003. Oxidation state of the active-site cysteine in protein tyrosine phosphatase 1B. *Nature.* 423:773–775.
33. Anstrom, D. M., K. Kallio, and S. J. Remington. 2003. Structure of the *Escherichia coli* malate synthase G:pyruvate:acetyl-coenzyme a abortive ternary complex at 1.95 Å resolution. *Protein Sci.* 12:1822–1832.
34. Davis, K., T. Foos, J. Wu, and J. V. Schloss. 2001. Oxygen-induced seizures and inhibition of human glutamate decarboxylase and porcine cysteine sulfinic acid decarboxylase by oxygen and nitric oxide. *J. Biomed. Sci.* 8:359–364.
35. Park, E., S. Y. Park, C. Wang, J. Xu, G. LaFauci, and G. Schuller-Levis. 2002. Cloning of murine cysteine acid decarboxylase and its mRNA expression in murine tissues. *Biochim. Biophys. Acta.* 1574:403–406.
36. Popescu, V. C., E. Münck, B. G. Fox, Y. Sanakis, J. G. Cummings, I. M. Turner, and M. J. Nelson. 2001. Mössbauer and EPR studies of the photoactivation of nitrile hydratase. *Biochemistry.* 40:7984–7991.
37. Payne, M. S., S. Wu, D. R. Fallon, G. Tudor, B. Stieglitz, I. M. Turner, and M. J. Nelson. 1997. A stereoselective cobalt-containing nitrile hydratase. *Biochemistry.* 36:5447–5454.
38. Chatel, S., M. Rat, S. Dijos, P. Leduc, J. P. Tuchagues, D. Mansuy, and I. Artaud. 2000. Toward model complexes of Co-containing nitrile hydratases: synthesis, complete characterization and reactivity toward ligands such as CN^- and NO of the first square planar Co^{III} complex with two different carboxamido nitrogens and two thiolato sulphur donors. *J. Inorg. Biochem.* 80:239–246.
39. Shoner, S. C., D. Barnhart, and J. A. Kovacs. 1995. A model for the low-spin, non-heme, thiolate-ligated iron site of nitrile hydratase. *Inorg. Chem.* 34:4517–4518.
40. Ellison, J. J., A. Nienstedt, S. C. Shoner, D. Barnhart, J. A. Cowen, and J. A. Kovacs. 1998. Reactivity of five-coordinate models for the thiolate-ligated Fe site of nitrile hydratase. *J. Am. Chem. Soc.* 120:5691–5700.
41. Shoner, S. C., A. M. Nienstedt, J. J. Ellison, I. Y. Kung, D. Barnhart, and J. A. Kovacs. 1998. Structural comparison of five-coordinate thiolate-ligated M^{II}=Fe^{II}, Co^{II}, Ni^{II} and Zn^{II} wrapped in a chiral helical ligand. *Inorg. Chem.* 37:5721–5726.
42. Jackson, H. L., S. C. Shoner, D. Rittenberg, J. A. Cowen, S. Lovell, D. Barnhart, and J. A. Kovacs. 2001. Probing the influence of local coordination environment on the properties of Fe-type nitrile hydratase model complexes. *Inorg. Chem.* 40:1646–1653.
43. Shearer, J., I. Y. Kung, S. Lovell, W. Kaminsky, and J. A. Kovacs. 2001. Why is an ''inert'' metal center in the active site of nitrile hydratase? Reactivity and ligand dissociation from a five-coordinate Co(III) nitrile hydratase model. *J. Am. Chem. Soc.* 123:463–468.
44. Shearer, J., H. L. Jackson, D. Schweitzer, D. K. Rittenberg, T. M. Leavy, W. Kaminsky, R. C. Scarrow, and J. A. Kovacs. 2002. The first example of a nitrile hydratase model complex that reversibly binds nitriles. *J. Am. Chem. Soc.* 124:11417–11428.
45. Lugo-Mas, P., A. Dey, L. Xu, S. D. Davin, J. Benedict, W. Kaminsky, K. O. Hodgson, B. Hedman, E. I. Solomon, and J. A. Kovacs. 2006. How does oxygen atom addition affect the properties of an Fe-nitrile hydratase analogue? The compensatory role of the unmodified thiolate. *J. Am. Chem. Soc.* 128:11211–11221.
46. Boone, A. J., M. G. Cory, M. J. Scott, M. C. Zerner, and N. G. J. Richards. 2001. Investigating the structural and electronic properties of nitrile hydratase model iron(III) complexes using projected unrestricted Hartree-Fock (PUHF) calculations. *Inorg. Chem.* 40: 1837–1845.
47. Mascharak, P. K. 2002. Structural and functional models of nitrile hydratase. *Coord. Chem. Rev.* 225:201–214.
48. Greene, N. S., C. H. Chang, and N. G. J. Richards. 2002. The role of post-translational modification in the photoregulation of Fe-type nitrile hydratase. *Chem. Commun.* 20:2386–2387.
49. Boone, A. J., C. H. Chang, S. N. Greene, T. Herz, and N. G. J. Richards. 2003. Modelling the spin-dependent properties of open-shell Fe(III)-containing systems: towards a computational description of nitrile hydratase. *Coord. Chem. Rev.* 238–239:291–314.
50. Chang, C., A. J. Boone, R. J. Bartlett, and N. G. J. Richards. 2004. Toward a computational description of nitrile hydratase: studies of the ground state bounding and spin-dependent energetics of mononuclear, non-heme Fe(III) complexes. *Inorg. Chem.* 43:458–472.
51. Harrop, T. C., and P. K. Mascharak. 2004. Fe(III) and Co(III) centers with carboxamido nitrogen and modified sulfur coordination: lessons learned from nitrile hydratase. *Acc. Chem. Res.* 34:253–260.
52. Silaghi-Dumitrescu, R. 2005. Nitrile hydration by the cobalt-containing nitrile hydratase. DFT investigation of the mechanism. *Revista de Chimie.* 56:359–362.
53. Dey, A., M. Chow, K. Taniguchi, P. Lugo-Mas, S. Davin, M. Maeda, J. A. Kovacs, M. Odaka, K. O. Hodgson, B. Hedman, and E. Solomon. 2006. Sulfur K-edge XAS and DFT calculations on nitrile hydratase: geometric and electronic structure of the non-heme iron active site. *J. Am. Chem. Soc.* 128:533–541.
54. Bishop, A. O. T., and T. Sewell. 2006. A new approach to possible substrate binding mechanisms for nitrile hydratase. *Biochem. Biophys. Res. Commun.* 343:319–325.
55. Greene, S. N., and N. G. J. Richards. 2006. Electronic structure, bonding, spectroscopy and energetic of Fe-depending nitrile hydratase active-site models. *Inorg. Chem.* 45:17–36.

56. Pepłowski, L., K. Kubiak, and W. Nowak. 2007. Insights into catalytic activity of industrial enzyme Co-nitrile hydratase. Docking studies of nitriles and amides. *J. Mol. Model.* 13:725–730.

57. Elber, R., and M. Karplus. 1990. Enhanced sampling in molecular dynamics: use of the time-dependent Hartree approximation for a simulation of carbon monoxide diffusion through myoglobin. *J. Am. Chem. Soc.* 112:9161–9170.

58. Noguchi, T., M. Nojiri, K. Takei, M. Odaka, and N. Kamiya. 2003. Protonation structures of Cys-sulfinic and Cys-sulfenic acids in the photosensitive nitrile hydratase revealed by Fourier transform infrared spectroscopy. *Biochemistry.* 42:11642–11650.

59. Suzuki, H., M. Nojiri, N. Kamiya, and T. Noguchi. 2004. Thermal equilibrium of two conformations in photosensitive nitrile hydratase probed by the FTIR band of nitric oxide bound to the non-heme iron center. *J. Biochem.* 136:115–121.

60. http://www.rcsb.org/pdb/home/home.do

61. Elber, R., C. Simmerling, R. Goldstein, H. Li, G. Verkhivker, C. Keasar, J. Zhang, and A. Ulitsky. 1995. MOIL: a program for simulations of macromolecules. *Comput. Phys. Commun.* 91:159–189.

62. Roitberg, A., and R. Elber. 1991. Modelling side chains in peptides and proteins: application of the locally enhanced sampling and the simulated annealing methods to find minimum energy conformations. *J. Chem. Phys.* 95:9277–9287.

63. Meller, J., and R. Elber. 1998. Computer simulations of carbon monoxide photodissociation in myoglobin: structural interpretation of the B states. *Biophys. J.* 74:789–802.

64. Kubiak, K., M. Kowalska, and W. Nowak. 2003. Molecular dynamics study of early events during photooxidation of eye lens protein γ B-crystallin. *J. Mol. Struct.* 630:315–325.

65. Simmerling, C., R. Elber, and J. Zhang. 1995. MOIL-View—a program for visualization of structure and dynamics of biomolecules and STO—a program for computing stochastic paths. *In* Modelling of Biomolecular Structure and Mechanisms. A. Pullman, J. Jortner, and B. Pullman, editors. Kluwer Academic, Dordrecht, The Netherlands. 241–265.

66. Humphrey, W., A. Dalke, and K. Schulten. 1996. VMD—visual molecular dynamics. *J. Mol. Graph.* 14:33–38.

67. Verkhivker, G., R. Elber, and W. Nowak. 1992. Locally enhanced sampling in free energy calculations: application of mean field approximation to accurate calculation of free energy differences. *J. Chem. Phys.* 97:7838–7841.

68. Straub, J. E., and M. Karplus. 1991. Energy equipartitioning in the classical time-dependent Hartree approximation. *J. Chem. Phys.* 94: 6737–6739.

69. Ulitsky, A., and R. Elber. 1993. The thermal equilibrium aspects on the time dependent Hartree and the locally enhanced sampling approximation: formal properties, a correction and computational examples for rare gas clusters. *J. Chem. Phys.* 98:3380–3388.

70. Hixon, C., and R. A. Wheeler. 2001. Rigorous classical-mechanical derivation of a multiple-copy algorithm for sampling statistical mechanical ensembles. *Phys. Rev. E Stat. Nonlin. Soft Matter Phys.* 64:026701.

71. Hixon, C. A., J. Chen, Z. Huang, and R. A. Wheeler. 2004. New perspectives of multiple-copy mean-field molecular dynamics methods. *J. Mol. Graph. Model.* 22:349–357.

72. Hixon, C. A., and R. A. Wheeler. 2004. Practical multiple-copy methods for sampling classical statistical mechanical ensembles. *Chem. Phys. Lett.* 386:330–335.

73. Schulten, K., H. Lu, and L. Bai. 1997. Probing protein motion through temperature echoes. *In* Physics of Biological Systems: From Molecules to Species. H. Flyvbjerg, J. Hertz, M. H. Jensen, O. G. Mouritsen, and K. Sneppen, editors. Springer, Berlin, Heidelberg. 117–152.

74. Sugita, Y., and Y. Okamoto. 1999. Replica-exchange molecular dynamics method for protein folding. *Chem. Phys. Lett.* 314:141–151.

75. Powell, M. J. D. 1964. An efficient method for finding the minimum of a function of several variables without calculating derivatives. *Comput. J.* 7:155–162.

76. Piersma, S. R., M. Nojiri, M. Tsujimura, T. Noguchi, M. Odaka, M. Yohda, Y. Inoue, and I. Endo. 2000. Arginine 56 mutation in the β subunit of nitrile hydratase: importance of hydrogen bonding to the non-heme iron center. *J. Inorg. Biochem.* 80:283–288.

77. Voet, D., and J. G. Voet. 1995. Biochemistry, 2nd ed. John Wiley & Sons, New York.

78. Takarada, H., Y. Kawano, K. Hashimoto, H. Nakayama, S. Ueda, M. Yohda, N. Kamiya, N. Dohmae, M. Maeda, and M. Odaka. 2006. Mutational study on alphaGln90 of Fe-type nitrile hydratase from Rhodococcus sp. N771. *Biosci. Biotechnol. Biochem.* 70:881–889.

79. Cohen, J., A. Arkhipov, R. Braun, and K. Schulten. 2006. Imaging the migration pathways for O_2, CO, NO, and Xe inside myoglobin. *Biophys. J.* 91:1844–1857.

80. Orłowski, S., and W. Nowak. 2007. Oxygen diffusion in minihemoglobin from Cerebratus lacteus—a locally enhanced sampling study. *Theor. Chem. Acc.* 117:253–258.

81. Orłowski, S., and W. Nowak. 2007. Locally enhanced sampling molecular dynamics study of the dioxygen transport in cytoglobin. *J. Mol. Model.* 13:715–723.

82. Desai, L. V., and M. Zimmer. 2004. Substrate selectivity and conformational space available to bromoxynil and acrylonitrile in iron nitrile hydratase. *Dalton Trans.* 6:872–877.

83. Jin, H., I. M. Turner Jr., M. J. Nelson, R. J. Gurbiel, P. E. Doan, and B. M. Hoffman. 1993. Coordination sphere of the ferric ion in nitrile hydratase. *J. Am. Chem. Soc.* 115:5290–5291.

84. Tyler, L. A., J. C. Noveron, M. M. Olmstead, and P. K. Mascharak. 1999. Oxidation of metal-bound thiolato sulfur centers in Fe(III) and Co(III) complexes with carboxamido nitrogens and thiolato sulfurs as donors: relevance to the active sites of nitrile hydratases. *Inorg. Chem.* 38:616–617.

85. Tyler, L. A., J. C. Noveron, M. M. Olmstead, and P. K. Mascharak. 2003. Modulation of the pKa of metal-bound water via oxidation of thiolato sulfur in model complexes of Co(III) containing nitrile hydratase: insight into possible effect of cysteine oxidation in Co-nitrile hydratase. *Inorg. Chem.* 42:5751–5761.

86. Pepłowski, L., K. Kubiak, S. Zelek, and W. Nowak. 2008. A comparative DFT study of substrates and products of industrial enzyme nitrile hydratase. *Int. J. Quantum Chem.* 108:161–179.

87. Li, H., R. Elber, and J. E. Straub. 1993. Molecular dynamics simulation of NO recombination to myoglobin. *J. Biol. Chem.* 268:17908–17916.

88. Kubiak, K., and W. Nowak. 2007. Molecular dynamics in excited states: Landau-Zener model of nitric oxide geminate recombination to nitrile hydratase. *In* From Computational Biophysics to Systems Biology (CBSB07). *Proceedings of the NIC Workshop 2007.* U. H. E. Hansmann, J. Mohanty, and O. Zimmermann, editors. John von Neumann Institute for Computing, Julich, Germany, NIC Series. 36:259–262.